Low-energy electron collisions with tetrafluoroethene, C 2 F 4

C. Winstead and V. McKoy

Citation: The Journal of Chemical Physics **116**, 1380 (2002); doi: 10.1063/1.1429649
View online: http://dx.doi.org/10.1063/1.1429649
View Table of Contents: http://scitation.aip.org/content/aip/journal/jcp/116/4?ver=pdfcov
Published by the AIP Publishing

Low-energy electron collisions with tetrafluoroethene, C_2F_4

C. Winstead and V. McKoy
A. A. Noyes Laboratory of Chemical Physics, California Institute of Technology, Pasadena, California 91125

(Received 16 April 2001; accepted 31 October 2001)

We report calculated cross sections for elastic and inelastic collisions of low-energy electrons with tetrafluoroethene, C_2F_4. The elastic cross section shows a number of resonance features, which we classify according to symmetry and analyze in relation to available experimental data. Electron-impact excitation cross sections are obtained for the $1\,^3B_{1u}$ (T) and $1\,^1B_{1u}$ (V) states arising from the $\pi\rightarrow\pi^*$ transition, as well as for eight other low-lying excited states arising from excitations out of the highest occupied molecular orbital. As expected, the T and V states make the largest individual contributions to electron-impact excitation at low energies; however, the other states are shown to contribute significantly to the total excitation cross section at impact energies from 10 to 25 eV. © *2002 American Institute of Physics.* [DOI: 10.1063/1.1429649]

I. INTRODUCTION

Tetrafluoroethene (tetrafluoroethylene, perfluoroethylene, C_2F_4) has attracted interest as a feed gas in plasma etching of silicon dioxide[1,2] and is also formed within plasmas by dissociation of another common feed gas used for oxide etching, octafluorocyclobutane (c-C_4F_8).[3] Detailed understanding of the complex physical and chemical processes within a plasma reactor requires data describing the important collisional and reactive processes occurring both within the plasma and at the semiconductor surface. Among the many processes of interest, elastic and inelastic collisions between electrons and molecules of feed gas are particularly important, because such collisions are the principal mechanism of energy deposition, with the electrons serving to couple the applied fields to the internal and translational modes of the heavy particles and, simultaneously, to create reactive species. Electron collisions with C_2F_4 are also of considerable fundamental interest. C_2F_4 is the perfluoro analogue of the much-studied ethene molecule, and past studies have often considered C_2F_4 as a member of the fluoroethene series $C_2H_xF_{4-x}$. C_2F_4 is moreover significant as one of the simplest of the perfluorocarbons, which as a group have received considerable recent attention.

However, surprisingly little work, experimental or theoretical, has yet been done on electron collisions with C_2F_4. Electron-impact ionization, including ionic fragmentation, has been studied by Mohler *et al.*,[4] by Lifshitz and Long,[5–8] and most recently by Haaland and Jiao,[9] who, in contrast to the earlier studies, determined absolute ionization cross sections over a wide energy range. Dissociative attachment was studied by Morrison,[10] by Thynne and MacNeil,[11] by Heni *et al.*,[12] and by Illenberger *et al.*[13] Dissociative attachment can give valuable insight into the existence and location of scattering resonances, although resonance peaks seen in attachment will typically be shifted lower in energy, due to lifetime effects, compared to the same resonances in the elastic or total scattering cross sections.[14] A direct search for resonances in the C_2F_4 cross section was undertaken by Chiu *et al.*[15] using electron transmission spectroscopy; their technique measures the derivative of the total cross section, rather than the cross section itself, and is thus sensitive to rapid variations with energy caused by sharp resonances (though it may fail to see weak or broad features). Coggiola *et al.*[16] measured the excitation threshold energies for several states and obtained relative differential cross sections for elastic scattering and for two excitation processes at 25 and 40 eV. Their limited data appear to be the only elastic or electron-impact excitation cross sections for C_2F_4 available to date. At energies of 30–3000 eV, Jiang *et al.*[17] computed total cross sections for electron–C_2F_4 scattering using simple models. We are not aware of other theoretical cross sections.

In the present work, we report differential, integral, and momentum-transfer cross sections for elastic scattering of low-energy electrons by C_2F_4, as well as differential and integral cross sections for 10 electron-impact excitation channels, all computed using the Schwinger multichannel (SMC) variational method.[18,19] As in C_2H_4, the $\pi\rightarrow\pi^*$ excitations involving the highest occupied and lowest unoccupied molecular orbitals, producing the T (triplet) and V (singlet) states of Mulliken, are of particular interest and make the greatest contributions to the neutral-excitation cross section; however, we find that other low-lying excitation processes make, in aggregate, a significant contribution to the total excitation cross section over a certain energy range. We examine the resonance structure in the cross sections and relate our work to previous studies.

A summary account of the integral cross sections obtained from the present work is given elsewhere.[20]

II. COMPUTATIONAL DETAILS

The collision calculations were carried out using the Schwinger multichannel (SMC) variational method[18,19] as implemented for parallel computers.[21,22] Details may be found in the references cited. Here we describe only the features particular to the present calculations.

We will use Mulliken's convention[23] for associating orbitals of C_2F_4 with irreducible representations of D_{2h}. Accordingly, the highest occupied molecular orbital (the C–C π

TABLE I. Calculated properties of the lowest excited states of C_2F_4.

State	Energy (eV) IVO	Energy (eV) SECI	Oscillator strength (SECI)
$1\,^3B_{1u}$ (T)	5.03	4.48	0.0
$1\,^3B_{1g}$	7.10	6.76	0.0
$1\,^3B_{3u}$	7.29	7.17	0.0
$1\,^1B_{1g}$	7.83	7.55	0.0
$1\,^1B_{3u}$	8.03	7.74	0.0545
$1\,^3B_{2g}$	8.83	8.55	0.0
$1\,^3A_g$	9.02	8.95	0.0
$1\,^1B_{2g}$	9.59	9.21	0.0
$1\,^1A_g$	9.22	9.21	0.0
$1\,^1B_{1u}$ (V)	11.24	9.71	0.6308

bonding orbital) is labeled $1b_{3u}$, while the lowest unoccupied (π^*) orbital is $1b_{2g}$. The T and V states that are of primary interest are therefore $(1b_{3u}\rightarrow 1b_{2g})$ $1\,^3B_{1u}$ and $(1b_{3u}\rightarrow 1b_{2g})$ $1\,^1B_{1u}$, respectively. To identify additional excitations of interest, we performed a single-excitation configuration–interaction (SECI) calculation using GAUSSIAN[24] and its internal 6-311+G($3d$) basis set. Results of this calculation are shown in Table I. We choose to carry out electron collision calculations for the eight states besides the T state that have thresholds below the V state threshold: the $1\,^{1,3}B_{1g}$, $1\,^{1,3}B_{3u}$, $1\,^{1,3}B_{2g}$, and $1\,^{1,3}A_g$ states. Like the T and the V states, each of these states arises, in a one-electron picture, from excitation out of the $1b_{3u}$ orbital. As shown in Table I, of all the states considered, only the V state has a large optical oscillator strength; indeed, all but one of the other singlet transitions (and, of course, all of the triplet transitions) are forbidden by dipole selection rules.

All calculations were carried out at the experimental nuclear geometry of the ground electronic state.[25] For the elastic calculations, the 6-311+G($3d$) basis set internal to GAMESS,[26] with default splitting factors for the d functions, was used to construct the target wave functions. The same basis set was used for calculating the excitation cross sections of the T and V states. For comparison purposes, we also computed elastic, T state, and V state cross sections using the internal triple-zeta valence (TZV) basis set of GAMESS together with one diffuse s, one diffuse p, and two d functions, again with default splitting factors; we will refer to this as the TZV+($2d$) basis set. Because both GAMESS and the SMC program retain all six Cartesian components of the d functions, the total number of one-electron basis functions was 210 in the 6-311+G($3d$) basis set and 180 in the TZV+($2d$) basis set. We found only minor differences between the TZV+($2d$) and 6-311+G($3d$) results: The elastic and V state cross sections at higher energies were somewhat larger using the 6-311+G($3d$) basis, while peaks in the cross section for the T state at lower energies were somewhat stronger using the TZV+($2d$) basis. Because of the close agreement between the two sets of results, we used the smaller TZV+($2d$) basis set to compute cross sections for the remaining excitations. The doublet configuration state functions making up the variational basis sets in the scattering calculations were formed within the respective one-electron bases by combining singlet and triplet target states with virtual molecular orbitals.

The ground state of C_2F_4 was described by a self-consistent-field (SCF) wave function, while excited states were described within the improved virtual orbital (IVO) approximation,[27] a restricted form of SECI in which excitation takes place out of only one orbital, permitting a single-configuration description of the excited state. For purposes of the scattering calculations, the same target wave function was used to describe both the singlet and the triplet states arising from a given one-electron transition. The triplet IVO wave function was used for all but the $1\,^{1,3}A_g$ pair of states, for which generating the singlet IVO was easier due to technical factors. Examination of the principal configurations in the corresponding SECI wave functions indicates that considering the singlet and triplet wave functions to be identical is a very good approximation for the $^{1,3}B_{1g}$ and $^{1,3}A_g$ states and a reasonably good approximation for the remaining pairs of states. Additional information can be gained by comparing the SECI transition energies to the IVO transition energies in Table I. Based on an examination of the IVO orbitals, the $^{1,3}B_{1u}$ and $^{1,3}B_{1g}$ states are valencelike, the $^{1,3}B_{3u}$ states of $3s$ Rydberg character, the $^{1,3}B_{2g}$ states of $3p_z$ Rydberg character, and the $^{1,3}A_g$ states of $3p_y$ Rydberg character.

The elastic cross section was first computed at the static-exchange level of approximation. Further calculations incorporating polarization effects were then carried out for irreducible representations exhibiting prominent shape resonances, namely, $^2B_{1u}$, $^2B_{2g}$, and $^2B_{2u}$. A compact description of polarization was obtained by considering only symmetry-preserving virtual excitations in the presence of a resonancelike orbital, as described elsewhere;[28] for the $^2B_{1u}$ representation, which exhibits two shape resonances, we employed two such resonancelike orbitals. In the totally symmetric ^2A_g representation, the static-exchange approximation produces, as usual, a spurious s-wave enhancement of the cross section at the lowest energies. Redressing this behavior requires a highly accurate treatment of polarization, which can be computationally expensive, and which we did not carry out. In order to obtain more realistic cross sections for plasma-modeling purposes, however, we did make an *ad hoc* adjustment to the integral cross section by subtracting $24\exp(-0.4\times E^{1.25})\times 10^{-16}\,\mathrm{cm}^2$ (E in eV), which has the effect of bringing the ^2A_g component of the integral cross section smoothly down toward zero. Although this adjustment must fail at the lowest energies (the cross section should, in fact, be nonzero at $E=0$), it is reasonable as a first rough correction because we expect the cross section of C_2F_4, like that of related molecules such as C_2H_4 (Ref. 29) or C_2F_6,[30] to reach a small minimum value at an energy $\lesssim 1$ eV. Both the adjusted and the unadjusted results in A_g symmetry will be presented below.

The inelastic cross sections were obtained in a three-channel approximation, coupling the elastic channel in succession with the singlet and triplet channels arising from each different one-electron transition. To obtain results for the T state below the V state threshold, we also carried out a two-channel calculation in which the elastic and T-state channels were open, while the V-state excitation was in-

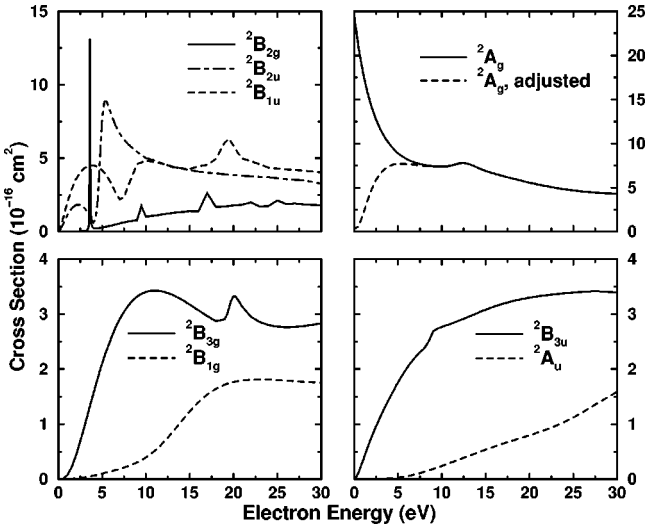

FIG. 1. Symmetry components of the integral elastic cross section for electron scattering by C_2F_4. See text for discussion.

cluded as a closed channel in generating the variational trial function.

Because excitation of the V state is strongly allowed under optical selection rules, it is important to include in the SMC calculation a correction for long-range (high partial wave) scattering. The procedure, which relies on the first Born approximation to scattering by a point (transition) dipole, has been described elsewhere.[31,32] In making this correction, we employed a transition dipole moment of 1.882 atomic units, computed with the b_{2g} IVO orbital of the $1\,^3B_{1u}$ state, and retained partial waves up to $l=6$, $m=4$ from the SMC calculation.

All collision calculations were carried out on a cluster of dual-processor Pentium II/300 MHz workstations connected over a gigabit Ethernet switch, using eight workstations as a 16-processor virtual parallel computer. Pre- and post-processing was also done on Pentium II/300 MHz workstations.

III. RESULTS AND DISCUSSION

A. Elastic scattering

Figure 1 shows the symmetry components of the integral elastic cross section of C_2F_4. As discussed in the preceding section, the $^2B_{1u}$, $^2B_{2g}$, and $^2B_{2u}$ components were obtained in the static-exchange plus polarization approximation, and the remaining components in the static-exchange approximation. Because polarization is most important at low energies (roughly, below 10 eV) and in the presence of resonances, its neglect is not expected to have a significant effect on the $^2B_{1g}$, $^2B_{3g}$, $^2B_{3u}$, or ^2A_u components, which are quite small at low energies and do not exhibit strong resonance features. For the ^2A_g component, which contains the contribution of the penetrating s-wave to the scattering amplitude, polarization is quite important at low energies. For the purpose of forming a more realistic estimate of the integral cross section, we empirically adjusted the ^2A_g component as described in Sec. II; Fig. 1 shows both the adjusted and the unadjusted values.

TABLE II. Observed dissociative-attachment maxima in C_2F_4.

Energy (eV)				
Ref. 10	Ref. 11[a]	Ref. 12	Ref. 13[a]	Anions observed[b]
2.8	3.6–4.3	3.0	3.0–4.3	F^-, CF_2^-, CF_3^-, $C_2F_3^-$
	4.9–5.4		5.0	F^-, F_2^-, $C_2F_3^-$
6.0	6.9–7.0	6.4	6.1–6.3	F^-, F_2^-, $C_2F_3^-$
11.6	11.5–11.9	11.5	11.5–11.9	F^-, CF^-

[a]Ranges are indicated where the peaks for different species fall at somewhat different energies.
[b]Not all anions listed are seen in each measurement. References 10 and 12 detect only F^-.

A striking feature in Fig. 1 is the sharp $^2B_{2g}$ resonance at 3.61 eV. (Sharp structures at higher energies in the $^2B_{2g}$ component are artifacts caused by treating as closed channels excitations that are in fact open channels at those energies.) This is the well-known π^* shape resonance seen at 3.00 ± 0.05 eV in electron transmission.[15] Dissociative attachment data are summarized in Table II; the strong F^- peak in the attachment cross section is placed variously at 2.8 to 3.6 eV, with recent work[12,13] giving a position of 3.0 ± 0.1 eV. It is important to observe that the extreme narrowness of the calculated resonance (full width at half maximum of 0.052 eV) is certainly an artifact of the fixed-nuclei approximation, both because the position of the resonance is expected to be sensitive to changes in molecular geometry and, more fundamentally, because the implied lifetime is greater than the vibrational period of several normal modes of C_2F_4. What we would expect to observe, therefore, is strong vibrational excitation via the resonance, with the vibrationally summed, electronically elastic cross section showing a broader feature with a smaller peak value.

The $C_2F_4^-$ ion is known to be stable, and experimental evidence points to a nonplanar structure.[33] Calculations[34–36] indicate that the lowest-energy conformation of the anion is the *anti* or ''chair'' structure of C_{2h} symmetry, with the two F atoms attached to one carbon bent downward from the plane of the neutral molecule while those attached to the other carbon are bent upward. The $^2B_{2g}$ resonance state can be expected to deform toward this structure, and one would thus expect the corresponding normal mode of C_2F_4 to be strongly excited. That the stable conformation of the anion is considerably distorted from the equilibrium geometry of the neutral may cause a downward shift in the observed resonance energy, helping to explain the $\sim$0.6 eV difference between our calculated resonance position and the position observed by Chiu *et al.*[15] Some of the difference may also be due to polarization effects not being fully represented in the model used, although that model has given good results in other cases.[28,37] Regardless of the precise location of the resonance, it is clearly much higher than 1.8 eV, which is the position of the π^* resonance in C_2H_4. The upward shift of the π^* resonance in the fluoroethenes has been discussed by Chiu *et al.*,[15] who suggest that shortening of the C–C and C–F bonds may be principally responsible.

A second strong shape resonance is found in $^2B_{2u}$ near 4.6 eV. Unlike the $^2B_{2g}$ resonance, the $^2B_{2u}$ resonance occurs in the presence of a strong nonresonant background, and

TABLE III. Minimal-basis-set (STO-6G) virtual orbitals of C_2F_4.

Symmetry	Energy (eV)	Principal character
b_{2g}	8.0	C–C π^*
b_{2u}	12.4	C–F σ^*
b_{1u}	14.9	C–F σ^*
a_g	16.6	C–F σ^*
b_{3g}	23.4	C–F σ^*
b_{1u}	25.9	C–C σ^*

the rapid eigenphase jump across the resonance profile gives rise, through interference with that background, to the highly asymmetric, window-and-peak resonance profile seen in Fig. 1. Employing a cubic polynomial (without a constant term) to represent the background $^2B_{2u}$ cross section from 0–12 eV and a Fano-type profile[38] to represent the resonant feature, we obtain from a nonlinear least-squares fit a resonance energy of 4.65 eV, a width of 1.16 eV, and a value for Fano's q parameter of 0.88. No clear experimental evidence for this resonance appears to exist. The electron transmission measurements of Chiu *et al.*[15] covered only the energy range containing the $^2B_{2g}$ resonance. As Table II shows, weak features are seen nearby in the attachment measurements of Thynne and MacNeil[11] and Illenberger *et al.*,[13] but the energy shift appears to be in the wrong direction (i.e., the attachment features lie above the elastic resonance). Despite the lack of a clear attachment signal, the resonance is so pronounced in the calculated cross section that it appears certain to have a detectable influence on scattering in the 4–5 eV energy range. Measurements of the total, elastic, or vibrational-excitation cross sections would help to establish or rule out its presence.

In $^2B_{1u}$ there are two resonances. The first occurs near 7.3 eV and has almost a pure window form, while the second appears as a fairly symmetric peak centered at about 19.4 eV. The 7.3 eV resonance may possibly be associated with the attachment peaks variously reported between 6 and 7 eV (Table II).

The remaining shape resonances visible in Fig. 1 occur at about 12.5 eV in ^2A_g and at about 20 eV in $^2B_{3g}$. Both are fairly broad. Because our calculation did not include polarization in either case, the actual resonance energies are likely to be somewhat lower, though the shift may be small owing to the relatively high energies and short lifetimes of these resonances. The ^2A_g resonance falls quite close in energy to dissociative attachment peaks that are seen at about 11.5 to 12 eV and appears to be the likely origin of those peaks.

It is instructive to compare the symmetries and energies of the resonances described above with those of the virtual valence molecular orbitals of C_2F_4. The symmetries of the virtual orbitals we may of course write down immediately by associating an antibonding orbital with each bonding orbital. The energies of the virtual orbitals are less well defined, but a Hartree–Fock calculation using a minimal basis set will generally provide useful qualitative information. Table III shows the results of such a calculation using the STO-6G minimal basis set internal to GAMESS.[26] As may be seen, there is a one-to-one correspondence between the resonances described above and antibonding valence orbitals of appropriate symmetry. Although the orbital energies are higher than the resonance positions by as much as 8 eV, the energy ordering is correct except in the case of the closely spaced $^2B_{1u}$ and $^2B_{3g}$ resonances near 20 eV.

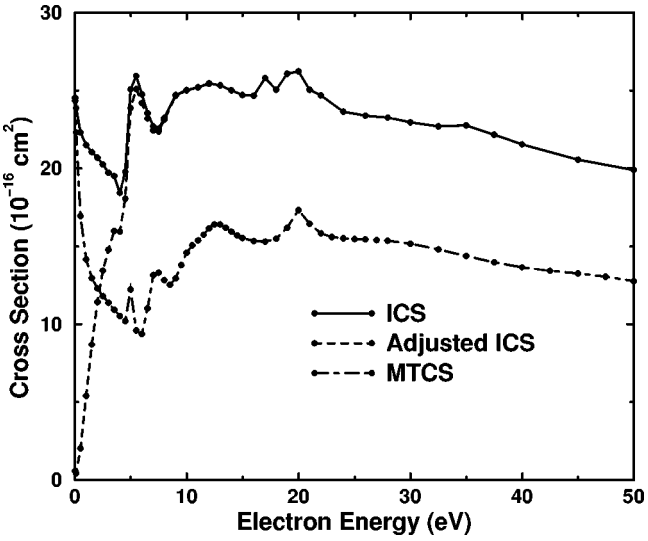

FIG. 2. Integral cross section (ICS) and momentum-transfer cross section (MTCS) for elastic scattering of electrons by C_2F_4. See text for discussion.

Figure 2 shows the integral cross section (ICS) obtained from the symmetry components of Fig. 1. Also shown in Fig. 2 is the momentum-transfer cross section (MTCS) computed in the static-exchange approximation. The $^2B_{2g}$ resonance is not fully resolved in the static-exchange MTCS and produces only a kink in the ICS, in both cases because of the relatively coarse spacing of points compared to the resonance width. As discussed above, the directly computed ICS is certainly too large at low energies, due to the incomplete representation of polarization, and an adjusted value in which the low-energy rise is suppressed is also shown in Fig. 2. The adjusted ICS should provide a better starting point for modeling. No experimental values of the ICS or MTCS appear to be available. The model-based total cross section of Jiang *et al.*[17] is about 50% larger than our computed elastic cross section from 30 to 50 eV. However, adding the excitation cross sections described below and the measured ionization cross section[9] to our elastic cross section produces an estimated total cross section that is only 20% to 25% larger than the elastic cross section over the same range.

Static-exchange differential cross sections (DCS) at selected energies are shown in Fig. 3. At 25 and 40 eV, we may compare to the measurements of Coggiola *et al.*,[16] which we have placed on an absolute scale by normalizing to our computed DCS at 25 eV and 30°. As may be seen, there is good qualitative agreement between the experimental and theoretical cross sections, and similar results would have been obtained from normalizing at any other angle except 20°, which would have raised the normalized values by about 30%. At 40 eV, the normalization we have chosen results in the calculated cross section falling below the experimental points at most angles, although the agreement at 20° is now fairly good.

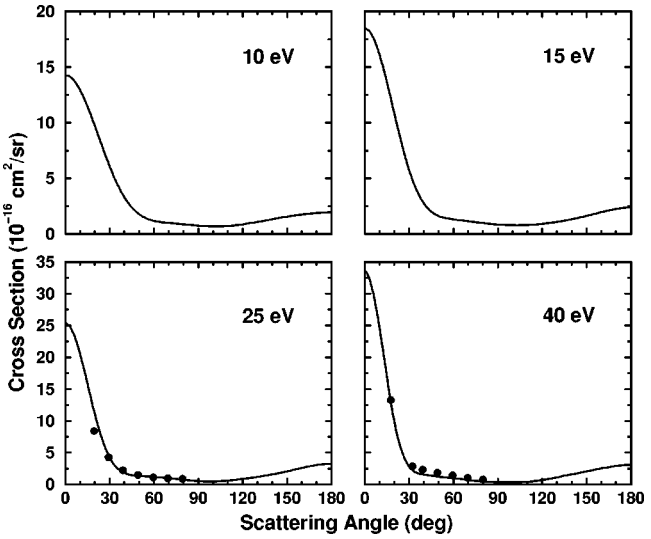

FIG. 3. Differential cross section for elastic scattering of electrons by C_2F_4 at selected energies. Solid line is the present calculation; circles are experimental data of Ref. 16, normalized to the calculated elastic cross section at 25 eV and 30°.

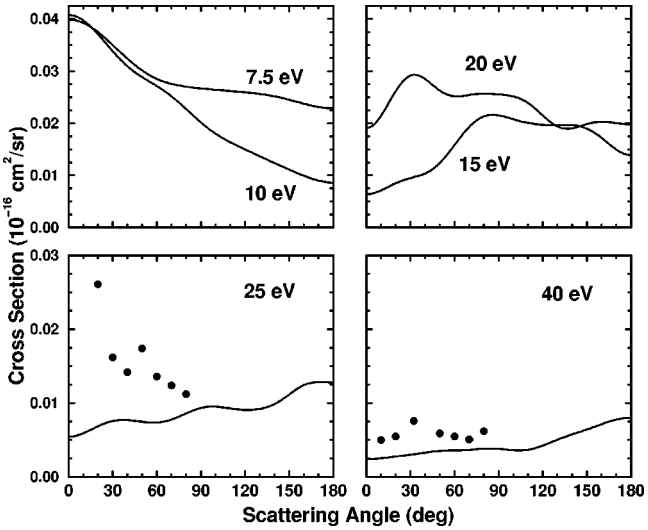

FIG. 5. Differential cross section for electron-impact excitation of the $1\,^3B_{1u}$ (T) state of C_2F_4 at selected energies. Symbols are as in Fig. 3.

B. *T* and *V* states

In Fig. 4 we show the integral excitation cross sections for the T ($1\,^3B_{1u}$) and V ($1\,^1B_{1u}$) states. As discussed in Sec. II, the T state cross section below the V state threshold is obtained from a separate calculation, giving rise to a discontinuity at the threshold for the V state. Corresponding differential cross sections are shown in Figs. 5 and 6, which also show, at 25 and 40 eV, the measured results of Coggiola *et al.*;[16] as just discussed, we have normalized their relative measurements by equating their elastic cross section at 25 eV and 30° to our ours.

Cross sections for spin-changing transitions typically fall off rapidly with energy, whereas cross sections for optically allowed excitations fall off slowly, as $\log(E)/E$. It is thus to be expected that the V state cross section should be much larger than the T state cross section at higher energies. However, as Fig. 4 shows, the V state cross section is considerably larger everywhere except very near the V-state threshold. Comparison of the calculated and measured cross sections in Figs. 5 and 6 shows that, although there is little agreement in detail, the order-of-magnitude agreement is reasonably good. There is, moreover, fair qualitative agreement between the calculated and measured results for the V state DCS (Fig. 6). Both exhibit the expected qualitative behavior for an optically allowed transition, the cross section displaying an increasingly sharp peak in the forward direction as the impact energy increases. For the T state, the experimental and calculated results do not agree even qualitatively at 25 eV; agreement is somewhat better at 40 eV, in the sense that both cross sections are more or less constant over the range of angles where comparison is possible. The calculated cross section for the T state shows the backward peaking at higher impact energies that is typical of singlet–triplet transitions.

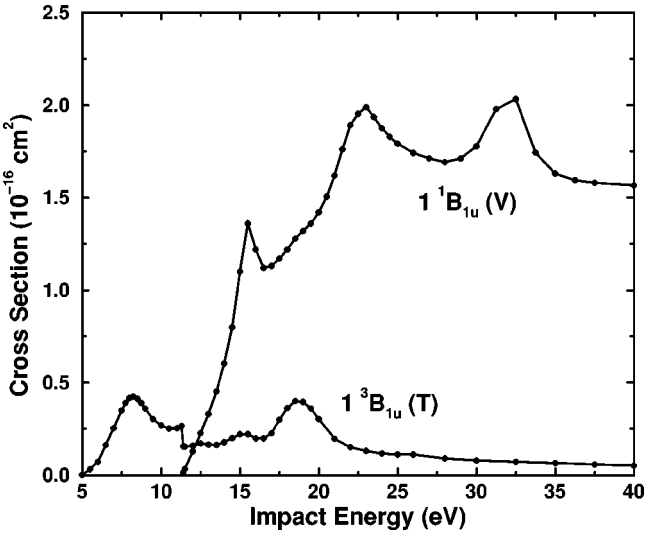

FIG. 4. Calculated integral cross sections for electron-impact excitation of the $1\,^3B_{1u}$ (T) and $1\,^1B_{1u}$ (V) states of C_2F_4.

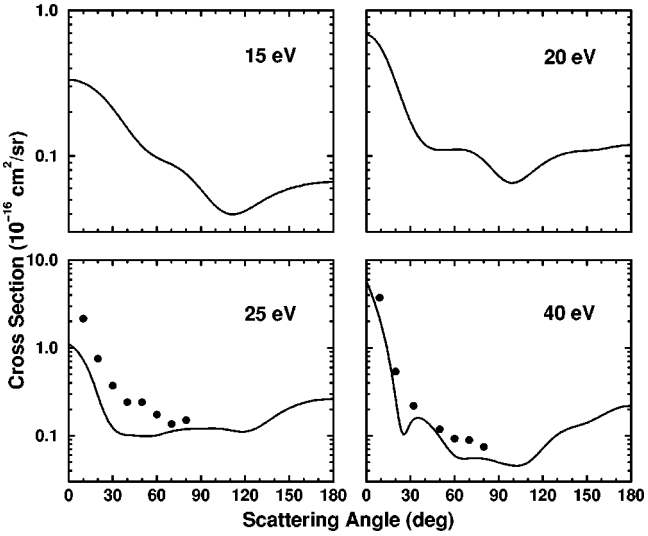

FIG. 6. As in Fig. 5, for the $1\,^1B_{1u}$ (V) state.

Before considering the possible resonance structure of the excitation cross sections, it should be emphasized that, as in the elastic cross section, the positions and widths of resonances are likely to change as the calculations are made more exact and the channel-coupling schemes expanded. As long as these limitations are borne in mind, however, symmetry assignment of features in the calculated cross section may provide at least a useful starting point in analyzing future experiments and calculations.

The cross sections for both the *T* and the *V* states display several local maxima. For the *T* state, the two most pronounced features, those near 8.2 eV and 19 eV, are both due to the $^2B_{1u}$ component of the cross section. A weaker maximum visible near 15 eV occurs in $^2B_{3u}$. One possible origin for such peaks is in core-excited shape resonances, that is, shape resonances formed in the field of the excited electronic state. From the B_{1u} spatial symmetry of the *T* state, we can deduce that the scattered wave associated with a $^2B_{1u}$ resonance must be a_g, while that associated with a $^2B_{3u}$ resonance is b_{2g}. A plausible assignment for one of the $^2B_{1u}$ peaks (probably that near 19 eV) is therefore a core-excited shape resonance involving either the C–F σ^* virtual valence orbital of a_g symmetry or the 3*s* Rydberg orbital. The peak near threshold is likely to be nonresonant, arising simply because the symmetry containing the *s* scattered wave ''turns on'' quickly above threshold. The symmetry of the peak near 15 eV is consistent with a core-excited shape resonance of either $(\pi^*)^2$ or $(\pi^*)^1(3d_{yz})^1$ type. As will be seen below, several other channels also display peaks near 15 eV associated with scattered waves of b_{2g} symmetry.

The sharp peak at 15 eV in the cross section for the *V* state occurs in $^2B_{3g}$ symmetry, implying a b_{2u} scattered wave. The broader peak near 23 eV has approximately equal contributions from $^2B_{3g}$ and ^2A_g, implying scattered waves of b_{2u} and b_{1u} symmetry, while another broad peak centered at about 32 eV contains nearly equal contributions from ^2A_g and $^2B_{2u}$, requiring scattered waves of b_{1u} and b_{3g} symmetry. There are also broad maxima in $^2B_{1u}$ centered near 18 and 25 eV, although these are not clearly visible in the summed *V*-state cross section of Fig. 4; these features are associated with a_g scattered waves. It is at least suggestive that the peaks between 23 and 32 eV correspond in number, general energy order, and scattered-wave symmetry with the σ^* valence virtual orbitals (Table III). If those peaks do indeed arise from core-excited resonances involving unoccupied valence orbitals, some other mechanism must account for the peaks at 15 and 18 eV. The sharp $^2B_{3g}$ peak at 15 is particularly puzzling. An alternative assignment that accounts for it would associate the $^2B_{3g}$ and ^2A_g peaks near 23 eV with 3*p* Rydberg resonances and the 15 eV peak with the b_{2u} C–F σ^* orbital. In either case, it is noteworthy and somewhat unexpected that no feature associated with a b_{2g} scattered wave is seen in the cross section for the *V* state, given that such features are found in the cross section for the *T* state and, as described below, for most other channels studied as well.

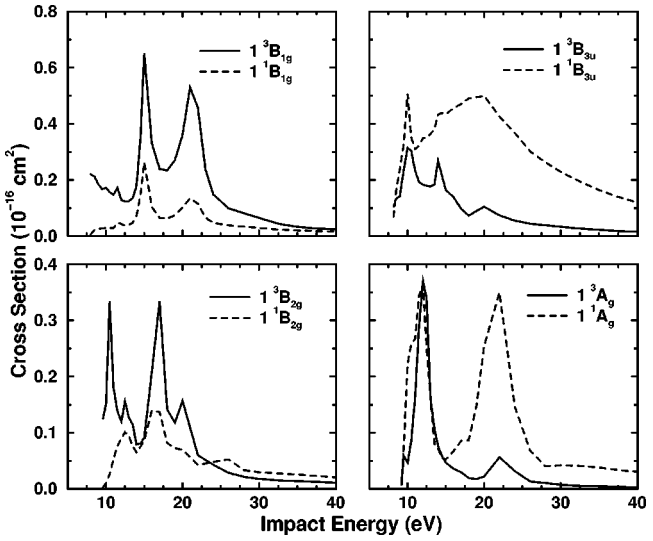

FIG. 7. Integral cross sections for electron-impact excitation of eight low-lying electronic states of C_2F_4.

C. Other excited states

Integral excitation cross sections for the remaining eight states of C_2F_4 that we studied are presented in Fig. 7. In almost all cases, the cross sections are small except within sharp peaks below 25 eV and die away rapidly at higher energy. The principal exception is the 1 $^1B_{3u}$ excitation, for which the cross section is smoother and remains relatively large over a wider energy range. It is almost certainly no coincidence that the 1 $^1B_{3u}$ transition is the only one among the eight shown in Fig. 7 that is optically allowed. Indeed, because we have not included the Born correction described in Sec. II for this transition as we did for the *V* state, the actual 1 $^1B_{3u}$ cross section should be even larger at higher energies than the uncorrected result shown in Fig. 7.

Decomposing the integral excitation cross sections into their symmetry components reveals that, in most cases, only a few components are important, and that, in general, the same components are important for both the triplet and the singlet states arising from a given one-electron transition. In both the 1 $^3B_{1g}$ and the 1 $^1B_{1g}$ cross sections, for example, the peaks near 15 and 21.5 eV arise from $^2B_{3g}$ symmetry, while the near-threshold scattering is dominated by $^2B_{2u}$. Likewise, the two most prominent peaks in the 1 $^3B_{2g}$ cross section, at about 10.5 and 17 eV, are both due to ^2A_g, and the same is true for the two strong peaks in the 1 $^1B_{2g}$ cross section near 12.5 and 16.5 eV. The 1 ^3A_g cross section is somewhat more complicated; the strong maximum near 13 eV is due primarily to ^2A_g, but $^2B_{1u}$ also contributes significantly, while the weaker maximum near 22 eV is due to $^2B_{3g}$ and $^2B_{1u}$. In the cross section of the corresponding ^1A_g state, the lower-energy maximum is dominated by $^2B_{1u}$, with a smaller contribution from ^2A_g, reversing the order seen in the triplet cross section. The higher-energy maximum is much larger than in the triplet cross section but, as in the triplet case, arises from overlapping $^2B_{3g}$ and $^2B_{1u}$ peaks, with $^2B_{3g}$ being stronger.

The 1 $^{1,3}B_{3u}$ excitations are a partial exception to the general rule stated in the first sentence of the preceding para-

graph. The $1\,^3B_{3u}$ cross section shows sharp peaks at about 10, 14, and 20 eV; the first of these is due to $^2B_{3u}$ and, to a lesser extent, $^2B_{1g}$, while the other two both occur in $^2B_{1u}$. Only one sharp peak is seen in the $1\,^1B_{3u}$ cross section, at 10 eV; this peak is due primarily to $^2B_{1g}$, which contributes to the corresponding peak in the triplet cross section, but also to ^2A_g. Although small peaks do exist in the $^2B_{1u}$ component of the singlet cross section near 14 and 20 eV, they are obscured by a broad background to which multiple symmetry components make contributions of comparable size, giving rise to the broad maximum between 15 and 25 eV.

If we analyze the cross section peaks not in terms of the overall symmetry of the doublet wave function for the electron–molecule system but instead in terms of the symmetry of the scattered wave, a clearer pattern emerges. In six of the channels—$1\,^{1,3}B_{1g}$, $1\,^{1,3}B_{3u}$, and $1\,^{1,3}B_{2g}$—there exists a pair of peaks for which the scattered wave has b_{2g} symmetry, and in four of these channels ($1\,^{1,3}B_{1g}$ and $1\,^{1,3}B_{2g}$) that pair of peaks dominates the cross section. One possible explanation for this observation is that the pairs of peaks arise from core-excited shape resonances built on the π^* valence orbital and the $3d_{yz}$ Rydberg orbital. However, it is also possible that these are pseudoresonances arising because the T and V states are not included as open channels in computing the cross sections of Fig. 7. Larger calculations with an extended channel-coupling scheme will be required to clarify the issue. In either case, it is unclear why the $1\,^{1,3}A_g$ cross sections should be exceptional in having no such marked features associated with a b_{2g} scattered electron.

If an explanation in terms of core-excited shape resonances is correct, the peaks not accounted for by the π^* and $3d_{yz}$ orbitals may be accounted for by orbitals of appropriate symmetry. For example, the $^2B_{1g}$ feature near threshold in the $1\,^{1,3}B_{3u}$ cross sections could arise from the b_{2u} valence virtual orbital (Table III). Again, however, more extensive calculations would be needed to make definite conclusions.

As noted earlier, our cross sections for the T and V states are smaller than the reported experimental values,[16] assuming (as seems likely) that no great error has arisen in normalizing the latter via the elastic cross section. On the other hand, one often finds that few-channel calculations overestimate the scattering cross section; to take a pertinent example, calculated cross sections[31,39] for the T and V states of C_2H_4 were about a factor of 2 larger than measured[40] values. Simulations[20,41] indicate that measured swarm parameters cannot be reproduced unless the total cross section for neutral excitation is larger than the sum of our cross sections for the T and V states, whereas including the cross sections for the additional eight states that we have calculated allows the simulated and measured swarm parameters to be brought into agreement, within experimental error. Possibly the calculated T and V cross sections are too low while the remaining calculated cross sections are too high, but it appears at least as likely that the measured T and V cross sections are too large. Clearly there is much room for measurements and more elaborate calculations to add insight.

IV. SUMMARY

We have reported low-energy electron cross sections for C_2F_4. Elastic cross sections computed within the static-exchange approximation, with polarization effects included in some symmetries where they are important. Electron-impact excitation cross sections were computed for 10 channels, including the T and V ($\pi\rightarrow\pi^*$) states as well as several other low-lying intravalence and Rydberg transitions. At 25 and 40 eV, differential cross sections for the elastic, T, and V channels could be compared to experimental data, which were placed on an absolute scale by a single-point normalization. Good agreement was found for the elastic cross sections; for both the T and the V states, order-of-magnitude agreement was found, in addition to fair qualitative agreement for the V state. Although the T and V states are most important to electron-impact excitation of C_2F_4, the remaining eight excitation channels were found to make a significant contribution to the total excitation cross section below 25 eV.

ACKNOWLEDGMENTS

This research was supported by Sematech, Inc., by the Office of Basic Energy Sciences of the Department of Energy, and by an equipment grant from Intel Corporation.

[1] S. Samukawa, T. Mukai, and K. Tsuda, J. Vac. Sci. Technol. A **17**, 2551 (1999).
[2] S. Samukawa and T. Mukai, Thin Solid Films **374**, 235 (2000).
[3] H. Hayashi, S. Morishita, T. Tatsumi, Y. Hikosaka, S. Noda, H. Nakagawa, S. Kobayashi, M. Inoue, and T. Hoshino, J. Vac. Sci. Technol. A **17**, 2557 (1999).
[4] F. L. Mohler, V. H. Dibeler, and R. M. Reese, J. Res. Natl. Bur. Stand. **49**, 343 (1952).
[5] C. Lifshitz and F. A. Long, J. Phys. Chem. **67**, 2463 (1963).
[6] C. Lifshitz and F. A. Long, J. Chem. Phys. **41**, 2468 (1964).
[7] C. Lifshitz and F. A. Long, J. Phys. Chem. **69**, 3731 (1965).
[8] C. Lifshitz and F. A. Long, J. Phys. Chem. **69**, 3737 (1965).
[9] P. D. Haaland (private communication).
[10] J. D. Morrison, Bull. Soc. Chim. Belg. **73**, 399 (1964).
[11] J. C. J. Thynne and K. A. G. MacNeil, Int. J. Mass Spectrom. Ion Phys. **5**, 329 (1970).
[12] M. Heni, E. Illenberger, H. Baumgärtel, and S. Süzer, Chem. Phys. Lett. **87**, 244 (1982).
[13] E. Illenberger, H. Baumgärtel, and S. Süzer, J. Electron Spectrosc. Relat. Phenom. **33**, 123 (1984).
[14] L. G. Christophorou, D. L. McCorkle, and A. A. Christodoulides, in *Electron-Molecule Interactions and Their Applications*, edited by L. G. Christophorou (Academic, Orlando, FL, 1984), p. 477, and references therein.
[15] N. S. Chiu, P. D. Burrow, and K. D. Jordan, Chem. Phys. Lett. **68**, 121 (1979).
[16] M. J. Coggiola, W. M. Flicker, O. A. Mosher, and A. Kuppermann, J. Chem. Phys. **65**, 2655 (1976).
[17] Y. Jiang, J. Sun, and L. Wan, Phys. Rev. A **62**, 062712 (2000).
[18] K. Takatsuka and V. McKoy, Phys. Rev. A **24**, 2473 (1981).
[19] K. Takatsuka and V. McKoy, Phys. Rev. A **30**, 1734 (1984).
[20] K. Yoshida, S. Goto, H. Tagashira, C. Winstead, V. McKoy, and W. L. Morgan, J. Appl. Phys. (to be published).
[21] C. Winstead and V. McKoy, Adv. At., Mol., Opt. Phys. **36**, 183 (1996).
[22] C. Winstead, C.-H. Lee, and V. McKoy, in *Industrial Strength Parallel Computing: Programming Massively Parallel Processing Systems*, edited by A. Koniges (Morgan-Kaufmann, San Francisco, 2000), p. 247.
[23] R. S. Mulliken, J. Chem. Phys. **66**, 2448 (1977).
[24] M. J. Frisch, G. W. Trucks, H. B. Schlegel *et al.*, GAUSSIAN 94, Revision C.4, Gaussian, Inc., Pittsburgh, PA, 1995.
[25] J. L. Carlos, R. R. Karl, and S. H. Bauer, J. Chem. Soc., Faraday Trans. 2 **70**, 177 (1974).

[26] M. W. Schmidt, K. K. Baldridge, J. A. Boatz, *et al.*, J. A. Montgomery, J. Comput. Chem. **14**, 1347 (1993).
[27] W. J. Hunt and W. A. Goddard, Chem. Phys. Lett. **3**, 414 (1969).
[28] C. Winstead and V. McKoy, Phys. Rev. A **57**, 3589 (1998).
[29] L. M. Brescansin, L. E. Machado, and M.-T. Lee, Phys. Rev. A **57**, 3504 (1998).
[30] L. G. Christophorou and J. K. Olthoff, J. Phys. Chem. Ref. Data **27**, 1 (1998).
[31] T. N. Rescigno and B. I. Schneider, Phys. Rev. A **45**, 2894 (1992).
[32] Q. Sun, C. Winstead, and V. McKoy, Phys. Rev. A **46**, 6987 (1992).
[33] M. C. R. Symons, J. Chem. Res., Synop. **1981**, 286 (1981).
[34] S. Merry and C. Thomson, Chem. Phys. Lett. **82**, 373 (1981).
[35] M. N. Paddon-Row, N. G. Rondan, K. N. Houk, and K. D. Jordan, J. Am. Chem. Soc. **104**, 1143 (1982).
[36] R. A. King, N. D. Pettigrew, and H. F. Schaefer, J. Chem. Phys. **107**, 8536 (1997).
[37] C.-H. Lee, C. Winstead, and V. McKoy, J. Chem. Phys. **111**, 5056 (1999).
[38] U. Fano, Phys. Rev. **124**, 1866 (1961).
[39] Q. Sun, C. Winstead, V. McKoy, and M. A. P. Lima, J. Chem. Phys. **96**, 3531 (1992).
[40] M. Allan, Chem. Phys. Lett. **225**, 156 (1994).
[41] W. L. Morgan (private communication).